Soil Dynamics and Earthquake Engineering 135 (2020) 106208

Contents lists available at ScienceDirect

Soil Dynamics and Earthquake Engineering

journal homepage: http://www.elsevier.com/locate/soildyn

Ground motion prediction equation for the Kathmandu Valley, Nepal based on strong motion records during the 2015 Gorkha Nepal earthquake sequence

Takuho Mori [a], Michiko Shigefuji [a,*], Subeg Bijukchhen [b], Tatsuo Kanno [a], Nobuo Takai [c]

[a] Faculty of Human-Environment Studies, Kyushu University, Fukuoka, Japan
[b] Department of Civil Engineering, Khwopa Engineering College, Bhaktapur, Nepal
[c] Faculty of Engineering, Hokkaido University, Sapporo, Japan

ARTICLE INFO

Keywords:
2015 Gorkha Nepal earthquake sequence
Long-period ground motion
Kathmandu Valley
Site amplification
Ground motion prediction equation
Bedrock depth

ABSTRACT

Single-site ground motion prediction equations (GMPEs) for the acceleration response spectra of each site in the Kathmandu Valley was constructed using strong motion records of magnitude 5.0 through 7.3 the 2015 Gorkha Nepal earthquake aftershocks observed at eight sites in the Kathmandu Valley. The regression coefficient for the site term has a strong correlation with the bedrock depth at each site in the Kathmandu Valley. Therefore, a new GMPE applicable to the whole Kathmandu Valley in the long-period range of 1–10 s was generalized using the bedrock depth as a parameter. We applied this GMPE to the largest aftershock. Consequently, at each sedimentary station, the residuals of the predicted value by GMPE are smaller than those predicted by the existing GMPE, and the peaks of the observed response spectra are reproduced well.

1. Introduction

The moment magunitude M_w 7.8 2015 Gorkha Nepal earthquake occurred in the Gorkha district, which is in the northwestern part of the capital city Kathmandu, Nepal, killed 8948 people, and caused damage to the World Heritage Sites in the Kathmandu Valley. The fault length and width are approximately 120 km and 80 km, respectively. The dip angle is low, and fault rupture extends from the epicenter to the east-southeast direction. The distance from the epicenter to central Kathmandu is approximately 80 km. However, the source fault reached just below Kathmandu. The depth of the source fault is approximately 10 km. Following the main shock, many aftershocks greater than M_w 5.0 occurred near the fault of the main shock. The largest aftershock of M_w 7.3 occurred in the northeast of Kathmandu.

Nepal is located on the Himalayan collision zone where the Indian plate and Eurasia plate collide, and at least seven earthquakes larger than M 7.5 have occurred in this zone since 1897 [1]. The 1934 Nepal-Bihar earthquake (M 8.3) was the largest earthquake, and caused serious damage as well as killing 8519 people in Kathmandu [2]. Moreover, Bilham et al. [3] pointed out the possibility of a mega-earthquake occurring in the Central Seismic Gap based on the occurrence interval of large earthquakes and stress accumulation in the Himalayan collision zone.

The Kathmandu Valley is covered with soft lake sediments [4], and the thickness is up to approximately 600 m. Since the basement topography of the basin is uneven [5], the sediment thickness varies greatly depending on the location of the valley. As strong motion is strongly affected by underground structure, understanding the ground motion characteristics in the Kathmandu Valley is significant. During the 2015 Gorkha earthquake, strong motions observed on sedimentary layers in the Kathmandu Valley were dominated by long-period ground motions with a period of 3–5 s due to the effect of the thick sedimentary layers [6–8]. In order to consider the cause of the long-period ground motion in Kathmandu Valley, Bijukchhen et al. [9] estimated one-dimensional S-wave velocity structure models under strong motion stations using observed records during aftershocks of the 2015 Gorkha earthquake. Additionally, Bijukchhen [10] constructed a three-dimensional velocity structure model. The difference of ground amplification characteristics at each site can be recognized.

A ground motion prediction equation (GMPE) is an equation that calculates seismic ground motion intensity, such as the response spectrum, including the characteristics of the source, path, and site effects. A GMPE is constructed by statistical regression analysis of many strong motion records. A GMPE is used for strong motion prediction over a

* Corresponding author.
E-mail address: shigefuji@arch.kyushu-u.ac.jp (M. Shigefuji).

https://doi.org/10.1016/j.soildyn.2020.106208
Received 29 September 2019; Received in revised form 28 March 2020; Accepted 1 May 2020
Available online 25 May 2020

Table 1
Earthquakes analyzed in the present study from USGS [17].

Event No.	Origin time (UTC)		M_w	Latitude (N)	Longitude (E)	Depth (km)	Data
1	2015/04/25	06:11:25	7.8	28.231	84.731	8.2	4
2	2015/04/25	06:45:21	6.6	28.224	84.822	10.0	4
3	2015/04/26	07:09:10	6.7	27.771	86.017	22.9	4
4	2015/04/26	16:26:06	5.0	27.830	85.865	14.0	4
5	2015/05/12	07:05:19	7.3	27.809	86.066	15.0	8
6	2015/05/12	07:36:54	6.3	27.625	86.162	15.0	8
7	2015/05/16	11:34:09	5.5	27.560	86.073	7.0	8

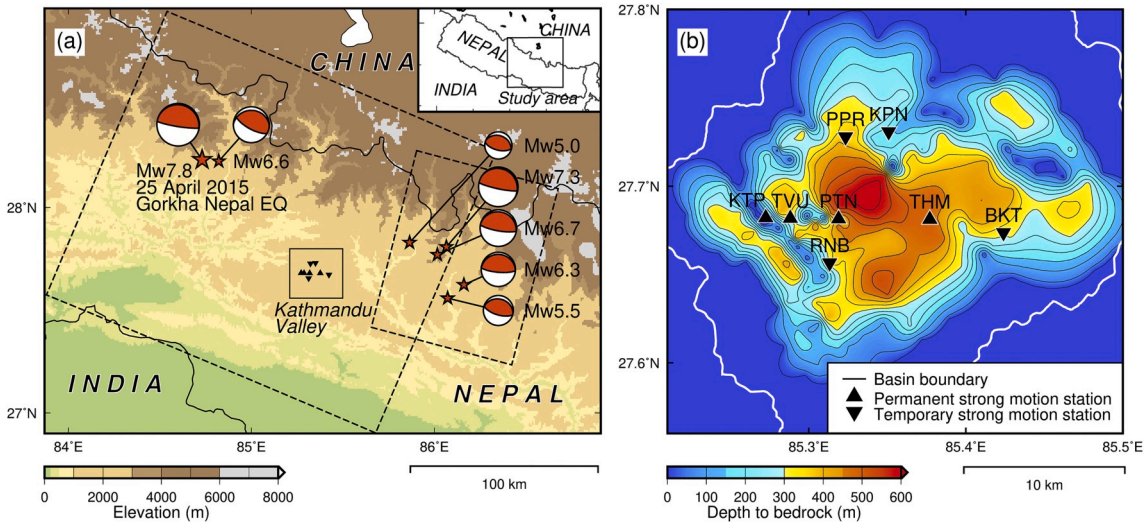

Fig. 1. (a) Epicenters of the main shock and aftershocks of the 2015 Gorkha earthquake and the source faults of the main shock (black dashed line) and the largest aftershock (red dashed line). Inset shows the location of the study area. Epicenters and focal mechanisms, fault planes were estimated by USGS [17] and Grandin et al. [18]. (b) Location of the strong motion stations [6,16] used in the present study and the bedrock depth distribution in the Kathmandu Valley [10]. (For interpretation of the references to color in this figure legend, the reader is referred to the Web version of this article.)

wide area because the average characteristics of strong motion can be obtained by a simple model. However, few GMPEs applicable to Kathmandu have been constructed because insufficient strong motion records have been accumulated in Nepal. Recently, the population and high-rise building have been increased in the Kathmandu Valley. The long-period GMPE is important for the Kathmandu Valley. As a previous study for Kathmandu, Singh et al. [11] constructed a GMPE using strong motion records of the 2015 Gorkha Nepal earthquake sequence observed at a strong motion observation network in India and one station in the central Kathmandu Valley. However, using records at only one sedimentary site is not appropriate for earthquake evaluation for the entirety of Kathmandu, which has complex sedimentary layer structures.

Thus, in the present study, we firstly investigate the ground motion characteristics individually at each site in the Kathmandu Valley, comparing strong motion records of the aftershocks of the 2015 Gorkha Nepal earthquake with existing GMPEs [12,13]. Next, we construct a single-site GMPE (SS-GMPE) [14] that predicts the acceleration response spectrum of each site in the Kathmandu Valley. Moreover, by generalizing the coefficients that related to the site effects and obtained at each site with the bedrock depth, the constructed GMPE is applicable to the whole Kathmandu Valley in the long-period range. Finally, we consider the applicability to the largest aftershock (M_w 7.3).

2. Database

We used instrument corrected acceleration records observed by the highly damped moving coil type strong motion seismometers (Mitsutiyo Corp. JEP-6A3-2) [15] installed at the Kathmandu Valley by Hokkaido University and Tribhuvan University: four permanent stations (KTP, TVU, PTN, and THM) installed on September 20, 2011, and four temporary stations (BKT, RNB, PPR, and KPN) installed from May to July 2015 [16]. Station KTP is located on a rock site, and the other stations are located on sediment sites. The 2015 Gorkha Nepal earthquake (M_w 7.8: event 1) and six of its aftershocks (between M_w 5.0 and 7.3: events 2 through 7), for which strong motion records were obtained at stations in the Kathmandu Valley, were used (Table 1). All events are inter-plate earthquakes in the collision zone with a low angle reverse fault focal mechanism, and the epicentral distance is approximately 60–80 km to Kathmandu. In the permanent stations, strong motion records of all events were obtained, and, at temporary stations, those of events 5 through 7 were obtained. Fig. 1a shows the epicenters of the main shock and aftershocks of the 2015 Gorkha Nepal Earthquake. The fault models of the 2015 Gorkha Nepal earthquake and the largest aftershock (M_w 7.3: event 5) are based on models by the United States Geological Survey [17] and by Grandin et al. [18], respectively. Fig. 1b shows the locations of the strong motion stations used in the present study and the bedrock depth distribution in the Kathmandu Valley [10]. At the same sedimentary stations, the sedimentary layers to the bedrock at PTN and THM appear to be thicker, while those at KPN appear to be thinner. In addition, TVU is located close to KTP, a station on the rock, and is surrounded by complex deep sedimentary layers.

3. Ground motion characteristics in the Kathmandu Valley

In order to focus on the long-period range, the pseudo-velocity response spectra at each station for the main shock and six aftershocks, as well as the site amplification factors of SH-wave at each site are shown in Fig. 2. These pseudo-velocity response spectra were obtained using the maximum of the vector sum of the horizontal-component response time histories with damping factor $h = 0.05$

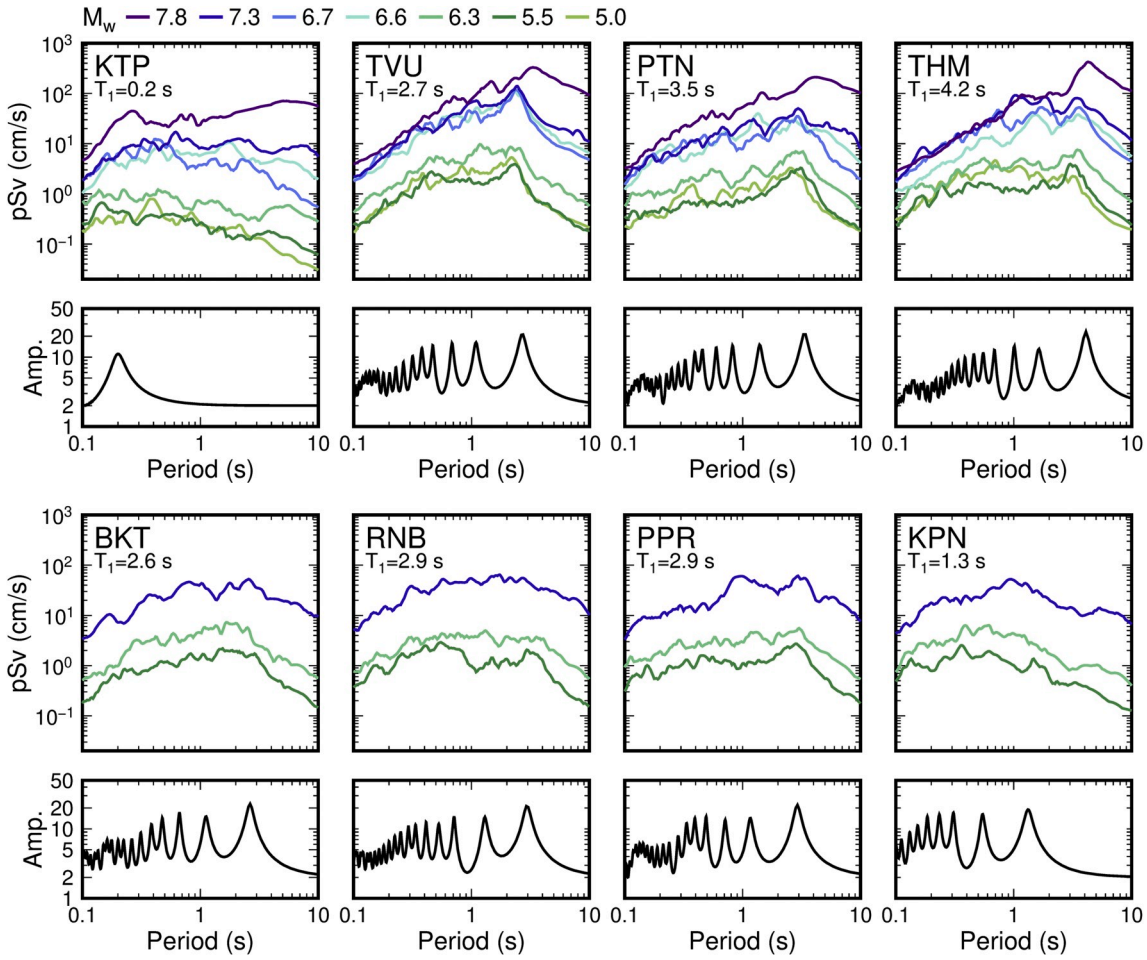

Fig. 2. Pseudo-velocity response spectra and SH-wave amplification factors [9] at each station. These pseudo-velocity response spectra were obtained by dividing the maximum values of the vector sum of the two horizontal-component response time histories with the damping factor ($h = 0.05$) for a specific natural period by the angular frequency. T_1 is a first peak period of the amplification factor.

divided by the angular frequency, the site amplification factor was calculated by the propagator matrix method [19] using the S-wave velocity structure under each station [9]. The *Q*-value was assumed to be one-tenth of the S-wave velocity for each layer. The strong motions of event 1 (M_w 7.8) at the sedimentary sites are affected by non-linear amplification of the ground. Therefore, the peak period shifts to a longer period compared to that for the weak motions of aftershocks. Rajaure et al. [20] also compared the response spectra of the 2015 Gorkha Nepal earthquake with the existing GMPEs [13,21] and suggested the existence of non-linear ground behavior during the main shock (M_w 7.8). From the above, these sites might be affected by non-linear ground behavior during sever strong ground motion. However, it is difficult to clarify the applicability and limitations of a GMPE for a huge earthquake, without a large number of records. Therefore, in the next chapter, we will construct the GMPE using only the data of the aftershocks (events 2 through 7) with peak ground acceleration less than 200 cm/s^2 that show linear ground behavior [e.g. Ref. [22,23]]. In events 2 through 7, the peaks are unclear at KTP on the rock site, while each site on the sediment layers has a peak with the same period in the long-period range. The peak period is widely distributed in the range of approximately 1.0–4.0 s. Compared with the amplification factor calculated from the one-dimensional S-wave velocity profile [9], the long-period peaks observed at the sedimentary sites correspond to the theoretical values. These amplifications are affected by high velocity contrast at the bedrock depth. Thus, the pseudo-velocity response spectra reflect the site effect of the sedimentary sites, and the ground amplification characteristic differs greatly at each site in the Kathmandu Valley.

We compared the observed and predicted pseudo-velocity response spectra using existing GMPEs in order to grasp the attenuation characteristics of the inter-plate earthquake in the collision zone in the Kathmandu Valley. Since few equations were available for the inter-plate earthquake in the collision zone, the following two equations for different earthquake types were selected for comparison.

The first GMPE was reported by Morikawa and Fujiwara [12]. This GMPE is for the 5% damped acceleration spectra and updated the strong motion database of Kanno et al. [24], including strong motion records observed in Japan from 1968 to 2011, in California, the United States, and in Turkey. The target earthquake category is the inter-plate earthquake in the subduction zone plate. We used the model for M_w 5.5 thorough 8.0 (equation (5) Model 2 of Morikawa and Fujiwara [12]). In the present study, we apply the model also to a M_w 5.0 event. The distance parameter is the shortest distance to the fault. Here, we used a correction term for shallow soft soils, and the average S-wave velocity of the uppermost 30 m soil (V_{S30}) is calculated from the S-wave velocity profiles reported by Bijukchhen et al. [9].

The second GMPE was reported by Boore et al. [13] and was developed as a part of the "Next Generation of Ground Motion Attenuation Models Project" for shallow crustal earthquakes in the United States. The database also includes the 1999 Chi-Chi Taiwan earthquake, which was an inter-plate earthquake in the collision zone. This GMPE is for the 5% damped pseudo-spectral acceleration. The distance parameter is the shortest distance to the surface projection of the fault plane. The fault type used was reverse slip (*RS*). Here, V_{S30} is calculated using

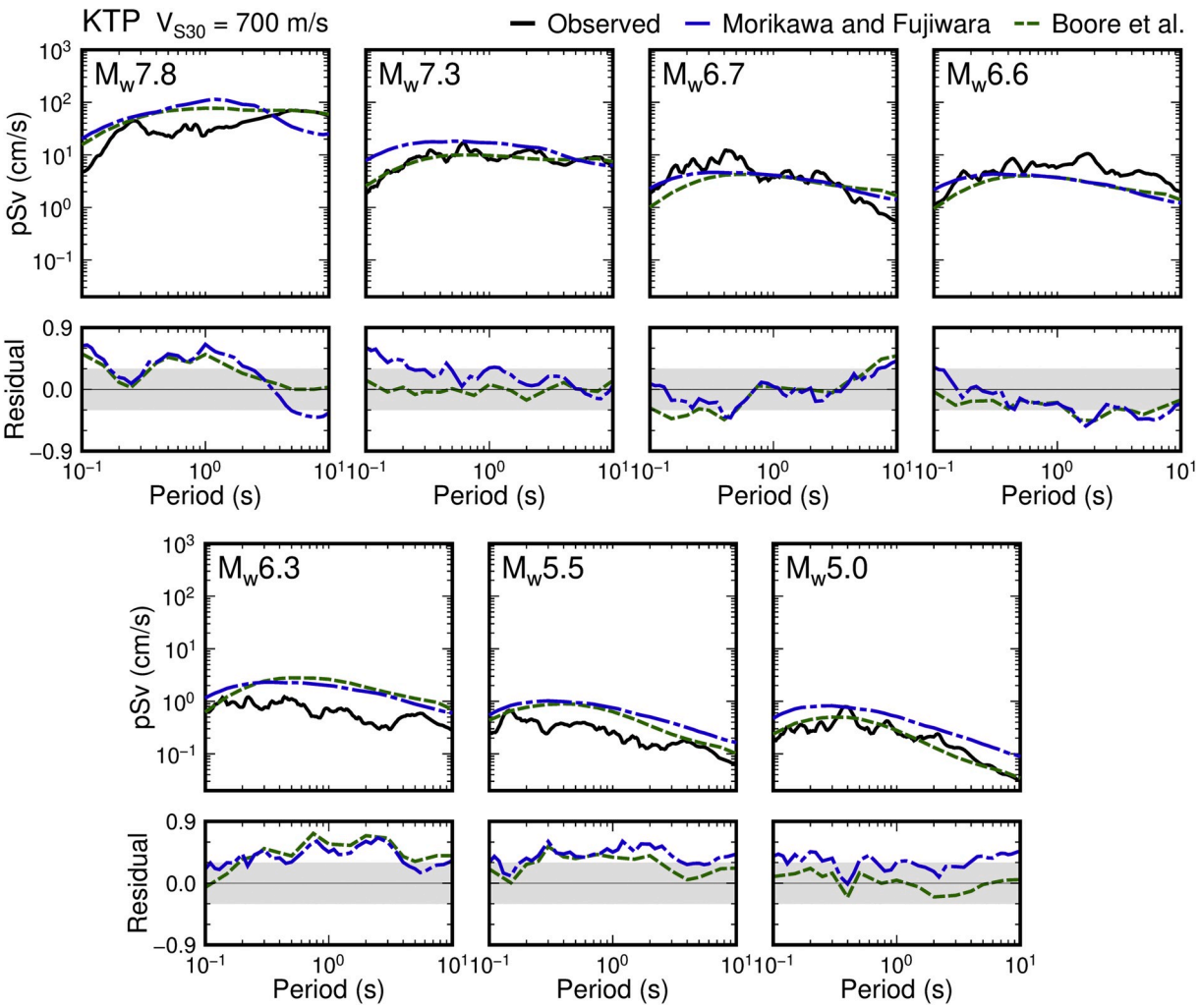

Fig. 3. Comparison of observed pseudo-velocity response spectra of events 1 through 7 at KTP (a station on the bedrock) and the corresponding records predicted by the two GMPEs [12,13] (upper) as well as the residuals (log [pre/obs]) (lower).

the same method as Morikawa and Fujiwara [12]. We used the default value of 0.0 as the regional coefficient Δc. In the case of an earthquake of $M_w > 7$, the distance parameters are calculated using fault models (Fig. 1). Otherwise, a hypocentral distance and an epicentral distance were used for the GMPEs of Morikawa and Fujiwara [12] and Boore et al. [13], respectively. Moreover, the correction term of the amplification by deep sedimentary layers are proposed by two GMPEs. These correction terms are expressed as the depth to the layer of S-wave velocity for 1400 m/s in Morikawa and Fujiwara [12], 1000 m/s in Boore et al. [13] respectively. Whereas S-wave velocity by Bijukchhen (2018) [10] used in the present study is 200, 300, 350, 400, 500, 700, 3200 m/s, there is no value corresponding to each parameter of both GMPEs. Therefore, we applied the top of the bedrock depth which is affected the amplification by deep sedimentary layers in the Kathmandu Valley instead of each parameter. For comparison, here, we used the pseudo-velocity response value converted from the acceleration response value by Morikawa and Fujiwara [12], and the velocity response spectrum from dividing the pseudo-acceleration response spectrum calculated from Boore et al. [13] by the angular frequency.

Fig. 3 shows the observed pseudo-velocity response spectra of events 1 through 7 at station KTP on the rock site and those predicted by the two GMPEs. The residuals, which are the differences between the predicted and observed values, are also shown. We defined the acceptable residual range as the observed value ± 0.3, which is a common logarithm of 1/2 to 2 times the observed value in the present study. At KTP on the rock site with a relatively small influence of the site effect, the predicted values by the two GMPEs for all events are almost within the acceptable residual range. This suggested that the source and path effects of the two equations are applicable to the 2015 Gorkha earthquake sequence, which was an inter-plate earthquake in the collision zone. Fig. 4 shows the observed pseudo-velocity response spectra of event 5 (M_w 7.3) at all stations, as well as those predicted by the two GMPEs, and their residuals. At the sedimentary sites with a large site effect, the predicted values by the two GMPEs tend to underestimate in the long-period range of the peak period of each station of approximately 1.0–4.0 s. There are no significant changes in the correction of the amplification by deep sedimentary layers. Therefore, the effect of the sedimentary layer of the Kathmandu Valley is assumed not to be sufficiently reflected in the existing equations.

4. Construction of ground motion prediction equations

From the results of the previous section based on the strong motion of the rock site, we confirmed that the equations of Morikawa and Fujiwara [12] and Boore et al. [13] are applicable with regard to source and path effects in the Kathmandu Valley. In this section, we construct a GMPE that can take into account the site effects of the Kathmandu Valley based on the existing equations. As mentioned above, since the valley has a complex underground structure, the single-site GMPE that is derived through regression analysis of pseudo-velocity response spectra

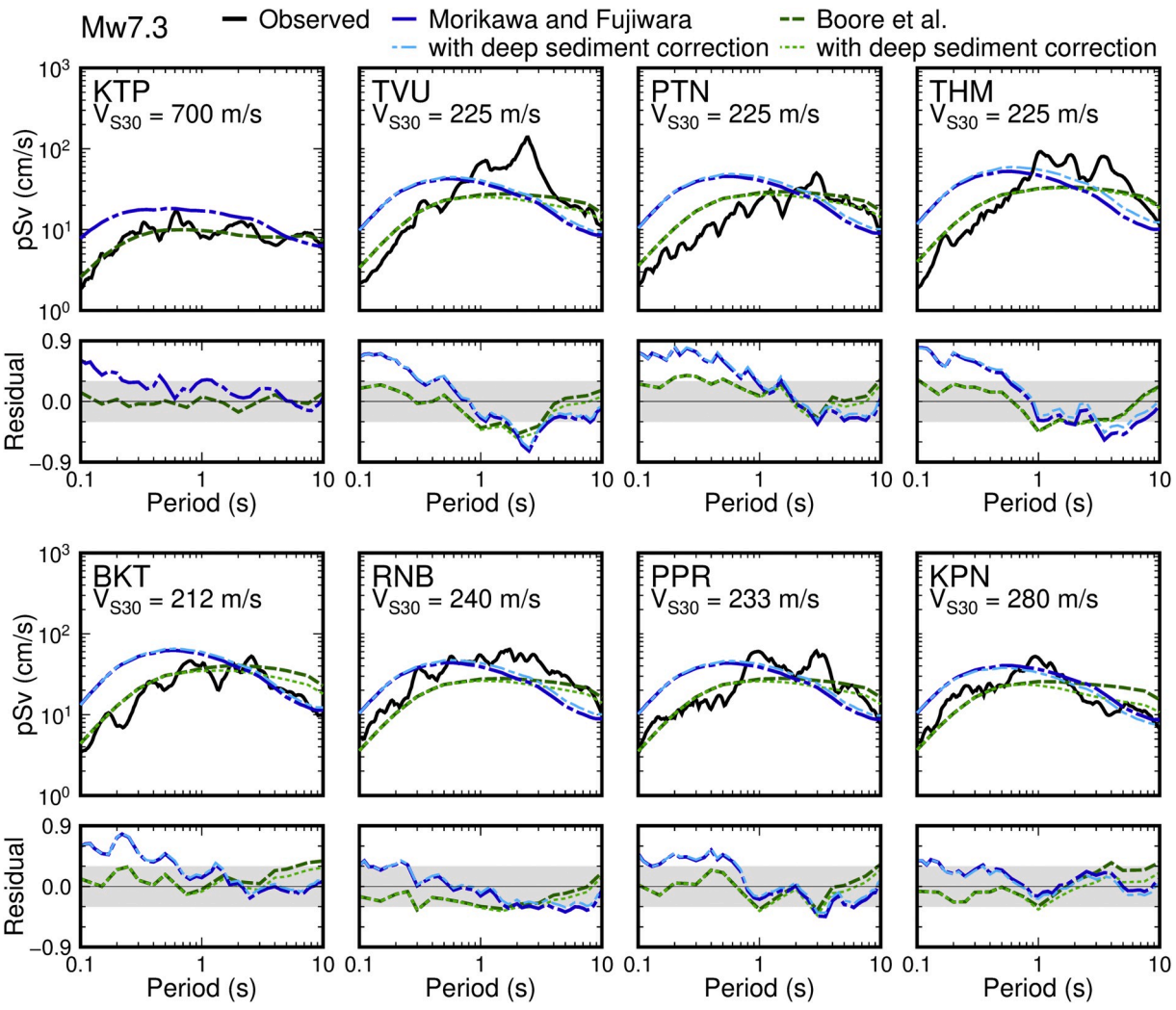

Fig. 4. Comparison of observed pseudo-velocity response spectra of event 5 (M_w 7.3) and the corresponding records predicted by the two GMPEs [12,13] (upper) and residuals (log [pre/obs]) (lower). Predicted values are shown also in the case that amplification by deep sedimentary layer is corrected.

calculated from multiple observed strong motion records at one site is constructed at first.

4.1. Single-site ground motion prediction equations

According to Fig. 2, the amplitude of the pseudo-velocity response spectra of other than the main shock (event 1; M_w 7.8), including the influence of nonlinearity at each site, tends to be correlated with the magnitude. In order to confirm this tendency, an example of the relationship between M_w and the response value at periods of $T = 0.1$, 0.3, 1.0, and 3.0 s is shown in Fig. 5. There is a linear relationship between the logarithm of the pseudo-velocity response value and M_w for any period range. Although the slope is different, the correlation coefficient shows a very high value. Therefore, we construct the SS-GMPE by regression analysis of the response value with M_w. In the present study, based on equation (5) Model 2 of Morikawa and Fujiwara [12] (equation (1)), which is a relatively simple model predicted for the acceleration response spectrum. We performed linear regression analysis using the least-squares method for the observed acceleration response spectra of events 2 through 7 with different M_w (equation (2)).

$$\log pre = a_2 M_w + b_2 X - \log\left(X + d_2 10^{0.5M_w}\right) + c_2 \quad (1)$$

where a_2 is the regression coefficient for the source term of the inter-plate earthquake in the subduction zone, b_2 and d_2 are those for the path anelastic attenuation term, c_2 is that for the site condition term, *pre* is the predicted 5% damped acceleration response spectra (*pre* in cm/s^2). In addition, X is the shortest distance from the source fault to a station (X in km).

$$aM_w + c_i = \log Obs_i - b_2 X + \log\left(X + d_2 10^{0.5M_w}\right) \quad (2)$$

where Obs_i, X are the same parameters as equation (1), and i indicates the number of the observation site (1–8). We thus obtain regression coefficients a for the source term and c_i for each site condition term. Coefficients b_2 and d_2 are the same as the values reported by Morikawa and Fujiwara [12]. Here, coefficient a is the average of the values obtained at each site. After regression analysis, coefficient c_i is calculated again using coefficient a. Table 2 and Fig. 6 show the coefficients of the newly constructed SS-GMPE.

From Fig. 6, coefficient a for the source term exhibits the same tendency as coefficient a_2 of the equation of Morikawa and Fujiwara, although the variation of an at each site is somewhat large for the period of 1–4 s. Hence, the equation of Morikawa and Fujiwara [12] for the inter-plate earthquake in the subduction zone is also applicable to the 2015 Gorkha Nepal earthquake sequence, which is the inter-plate earthquake in the collision zone. Coefficient c_i obtained by regression analysis mostly exhibits the same tendency at each site. However, a difference in period of more than approximately 1 s can be confirmed for each site.

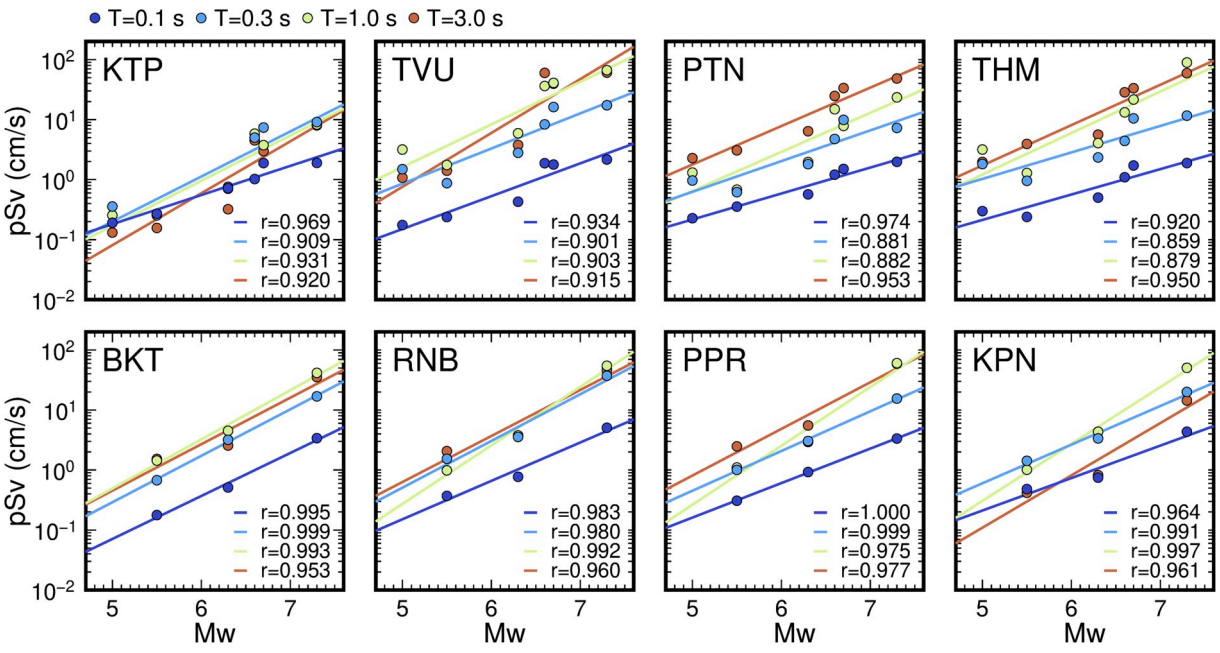

Fig. 5. Relationship between M_w and the response value at each site. The correlation coefficient and regression equation are shown, and the color corresponds to the natural period. The value of r is the correlation coefficient. (For interpretation of the references to color in this figure legend, the reader is referred to the Web version of this article.)

4.2. Ground motion prediction equation in the long-period range

The peak period in Fig. 6b appears to correspond to the natural period at each site shown in Fig. 2. Therefore, in order to consider the relationship between the peak period in Fig. 6b and the underground structure, Fig. 7a shows the difference between the coefficient c at sedimentary sites and that at KTP. In addition, Fig. 7b shows the relationship between the bedrock depth at each site in the Kathmandu Valley and the peak period for the difference between coefficient c on the sedimentary sites and that at KTP. Fig. 7 shows that coefficient c_i is large at the natural periods at each site. There is a correlation between the peak period and the sediment thickness at each site in the Kathmandu Valley [9]. Therefore, we generalize the coefficient c_i of SS-GMPE constructed in the previous chapter using the bedrock depth for constructing a GMPE applicable to the whole Kathmandu Valley. Fig. 8 shows the relationship between the coefficient c of each site at $T =$ 0.3, 0.5, 1.0, 3.0, 5.0 and 10.0 s and the bedrock depth ($Vs = 3200$ m/s) at each site. From Fig. 8, it can be seen that there is a strong linear correlation in the long-period range over 1.0 s. In Kathmandu Valley, the long-period ground motions are remarkable, so this result is considered significant for constructing a GMPE applicable to the whole Kathmandu Valley. From the above, we performed linear regression analysis using the least-squares method for the coefficient c of each site with the bedrock depth at each site in shown as equation (3).

$$c = pD_{3200} + q \ (\mathrm{T} = 1 - 10 \ \text{seconds}) \tag{3}$$

where p and q are the regression coefficient, c is the coefficient of a GMPE applicable to the whole Kathmandu Valley, and D_{3200} is the top of the bedrock depth at each site (D_{3200} in m; see supplementary information). Table 3 shows the coefficient p and q for determining c of the GMPE. On the other hand, for the period less than 1.0 s, it is necessary to consider another modeling such as using the shallow underground velocity structure as a parameter. However, since there is not enough of these structure data, the present study targets the long-period range.

Next, we verify the applicability of the GMPE constructed in the present study. Since strong motion data are limited, the data of event 5 (M_w 7.3) were used for verification of the regression analysis. Fig. 9 shows the observed and predicted pseudo-velocity response spectra of earthquake records at all stations, as well as the residuals. For comparision, the predicted values are acceleration spectra. therefore, the pseudo velocity will be reproduced with dividing by omega. At the sedimentary sites, the residuals of the values predicted by the present study are smaller than those predicted by the equation of Morikawa and Fujiwara [12], and the peaks of the observed pseudo-velocity response spectra are reproduced well.

Similarly, we constructed SS-GMPE based on Boore et al. [13] and confirmed that there was no difference between the predicted value based on two equations (see supplementary information).

5. Conclusion

In the present study, the ground motion characteristics of the Kathmandu Valley were discussed by comparing the pseudo-velocity response spectra of the aftershock records of the 2015 Gorkha Nepal earthquake observed in the valley with those obtained by existing GMPEs. Although the predicted values of the equations of Morikawa and Fujiwara [12] and Boore et al. [13] were within the acceptable residual range, at sedimentary sites, the predicted values of each site were significantly underestimated. This is due to the thick sedimentary layer covering the Kathmandu Valley, which gives different amplifications to the ground motion at each site. This amplification by the deep sedimentary structure, which is a feature of the Kathmandu Valley, could not be properly evaluated by existing GMPEs.

Therefore, we constructed the SS-GMPE, which considers the ground motion characteristics of each site in the Kathmandu Valley appropriately. The acceleration response spectra of the six aftershocks of the 2015 Gorkha Nepal earthquake were used to construct the SS-GMPE, and the regression equation based on an existing GMPE was regressed using M_w. As a result of applying the constructed SS-GMPE to the six aftershocks using regression analysis, the amplification characteristics at each site were appropriately evaluated. In addition, we confirmed that regression coefficient a related to the source effects in the present study exhibited the same tendency as the corresponding coefficient in the equation of Morikawa and Fujiwara [12]. Moreover, regression coefficient c related to the site effects differed by more than a period of approximately 1 s at each site. We calculated the difference between

Table 2
Regression coefficients a and c_i in shown as equation (2).

Period	a	c_{KTP}	c_{TVU}	c_{PTN}	c_{THM}	c_{BKT}	c_{RNB}	c_{PPR}	c_{KPN}
0.05	0.5411	0.3205	0.5293	0.3226	0.3774	0.1900	0.5291	0.3678	0.4897
0.06	0.5549	0.3045	0.4793	0.3186	0.3336	0.1532	0.5534	0.3889	0.4657
0.07	0.5411	0.5047	0.6003	0.4663	0.4767	0.3034	0.7302	0.5968	0.6473
0.08	0.5440	0.5546	0.6303	0.5315	0.4927	0.3717	0.7653	0.6411	0.7441
0.09	0.5460	0.6420	0.6527	0.6025	0.5292	0.4263	0.7866	0.7189	0.7660
0.10	0.5605	0.5818	0.5664	0.5623	0.4998	0.3561	0.6859	0.6309	0.6764
0.11	0.5513	0.6218	0.6150	0.6461	0.5777	0.4024	0.7013	0.8276	0.8040
0.12	0.5509	0.6401	0.6288	0.6849	0.5860	0.4024	0.7533	0.8104	0.9029
0.13	0.5357	0.7971	0.7459	0.7568	0.7281	0.5265	0.8641	0.9001	0.9941
0.15	0.5478	0.7358	0.6921	0.6981	0.6938	0.4827	0.8617	0.8146	0.8719
0.17	0.5815	0.4815	0.4750	0.4809	0.5181	0.3030	0.5728	0.4889	0.6527
0.20	0.5935	0.2563	0.4099	0.2742	0.3303	0.0705	0.3489	0.3229	0.4841
0.22	0.5744	0.3940	0.5349	0.3770	0.4616	0.2346	0.4580	0.4043	0.5493
0.25	0.5271	0.5920	0.8237	0.6519	0.8023	0.5270	0.8213	0.7209	0.8545
0.30	0.5816	0.1051	0.5234	0.2759	0.3648	0.1889	0.5390	0.3331	0.4096
0.35	0.5299	0.4214	0.8600	0.5771	0.6763	0.4778	0.7743	0.5340	0.7306
0.40	0.5237	0.4425	0.8919	0.5188	0.7074	0.4710	0.7178	0.4232	0.7353
0.45	0.5424	0.2108	0.7102	0.3084	0.5329	0.2751	0.5137	0.3533	0.4184
0.50	0.5447	0.0728	0.6201	0.2515	0.5042	0.1554	0.4906	0.2497	0.3931
0.60	0.5994	−0.3884	0.2475	−0.1454	0.1292	−0.2086	0.0958	−0.1721	0.0337
0.70	0.6102	−0.6313	0.0883	−0.2315	0.0121	−0.3185	−0.1137	−0.2949	−0.1811
0.80	0.6390	−0.9158	−0.1474	−0.6207	−0.3419	−0.5063	−0.3801	−0.5177	−0.4920
0.90	0.6843	−1.2976	−0.4523	−0.9190	−0.6830	−0.9018	−0.8078	−0.8778	−0.8187
1.00	0.7106	−1.5333	−0.6120	−1.1009	−0.8101	−1.1029	−1.0553	−1.0566	−1.0569
1.10	0.7194	−1.6602	−0.6880	−1.1266	−0.8727	−1.1872	−1.2323	−1.1457	−1.2305
1.20	0.7089	−1.6447	−0.7231	−1.0304	−0.8452	−1.2172	−1.1765	−1.1109	−1.2340
1.30	0.7060	−1.6528	−0.7324	−1.0218	−0.8810	−1.2601	−1.1432	−1.1372	−1.2674
1.50	0.6600	−1.4312	−0.4930	−0.9104	−0.6252	−0.9983	−0.8786	−0.9828	−1.0548
1.70	0.6950	−1.7314	−0.7265	−1.1398	−0.8753	−1.1592	−1.2763	−1.2900	−1.4322
2.00	0.6710	−1.6958	−0.5252	−0.9468	−0.8974	−1.1039	−1.1088	−1.1427	−1.4862
2.20	0.6767	−1.7517	−0.4987	−0.9647	−1.0146	−1.2255	−1.2279	−1.1852	−1.6447
2.50	0.6918	−1.9945	−0.6752	−1.0368	−1.1479	−1.3493	−1.4129	−1.2735	−1.8691
3.00	0.6965	−2.1537	−1.1499	−1.1085	−1.1160	−1.6207	−1.4077	−1.2821	−2.0389
3.50	0.7164	−2.3491	−1.5781	−1.4981	−1.2343	−1.9460	−1.6678	−1.6219	−2.2484
4.00	0.7456	−2.6070	−1.9014	−1.8405	−1.6239	−2.3234	−1.9496	−2.0698	−2.4888
4.60	0.8042	−3.0666	−2.4111	−2.3998	−2.2133	−2.7788	−2.5582	−2.6317	−2.9270
5.00	0.8543	−3.4138	−2.8167	−2.8031	−2.6387	−3.1833	−2.9643	−2.9941	−3.2718
5.50	0.8665	−3.5385	−2.9760	−3.0008	−2.8488	−3.3199	−3.1339	−3.1528	−3.4134
6.00	0.8938	−3.7528	−3.2293	−3.2617	−3.1403	−3.5801	−3.4222	−3.4198	−3.6674
6.50	0.9085	−3.9148	−3.3848	−3.4329	−3.3237	−3.7079	−3.6151	−3.6042	−3.8307
7.00	0.9167	−4.0412	−3.4883	−3.5506	−3.4530	−3.8162	−3.7246	−3.7278	−3.9220
7.50	0.9223	−4.1389	−3.5926	−3.6473	−3.5645	−3.9291	−3.8035	−3.8267	−3.9959
8.00	0.9190	−4.1626	−3.6197	−3.7010	−3.6151	−3.9905	−3.8337	−3.8690	−4.0354
8.50	0.9129	−4.1847	−3.6322	−3.7173	−3.6454	−4.0312	−3.8620	−3.9084	−4.0581
9.00	0.9024	−4.1751	−3.6267	−3.7224	−3.6370	−4.0246	−3.8779	−3.9029	−4.0565
9.50	0.8902	−4.1440	−3.5951	−3.7286	−3.6154	−3.9906	−3.8741	−3.9017	−4.0342
10.00	0.8774	−4.1154	−3.5565	−3.7018	−3.5882	−3.9465	−3.8604	−3.8792	−4.0077

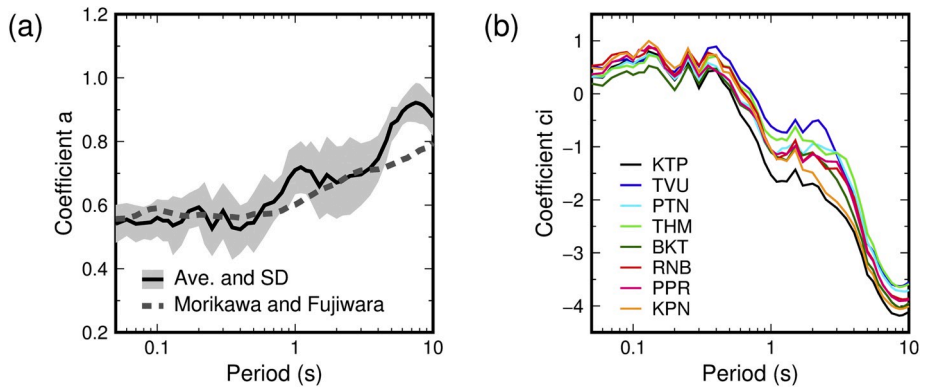

Fig. 6. (a) Average values of the regression coefficient *an* obtained at each site and coefficient a_1 used in the Morikawa and Fujiwara [12]. Error bars indicate standard deviations. (b) Constructed coefficient c_i at each site.

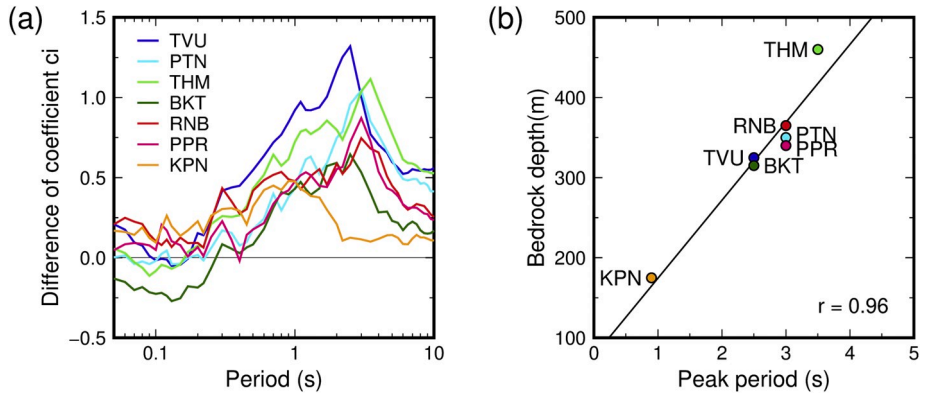

Fig. 7. (a) Difference between coefficient c_i at the sedimentary site and that at KTP. (b) Relationship between the bedrock depth at each site and the peak period of coefficient *c*. The correlation coefficient and regression equation are shown. The value of *r* is correlation coefficient.

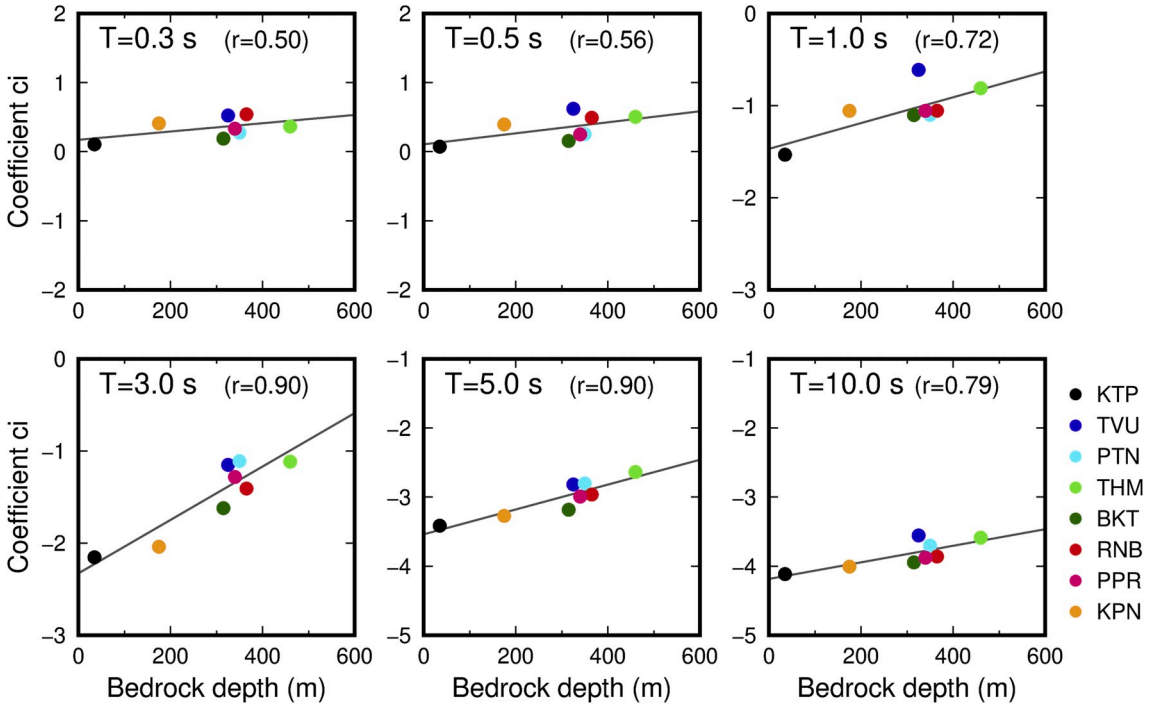

Fig. 8. Relationship between the coefficient *c* of each site at $T = 0.3$, 0.5, 1.0, 3.0, 5.0 and 10.0 s and the bedrock depth ($Vs = 3200$ m/s) at each site. The correlation coefficients and regression equations are shown. The value of *r* is correlation coefficient.

Table 3
Coefficient p and q for deerminingc in shown as equation (3).

Period	p	q
1.00	0.0014	−1.4695
1.10	0.0016	−1.6260
1.20	0.0017	−1.6302
1.30	0.0017	−1.6463
1.50	0.0017	−1.4361
1.70	0.0019	−1.7647
2.00	0.0021	−1.7460
2.20	0.0022	−1.8259
2.50	0.0025	−2.0804
3.00	0.0029	−2.3284
3.50	0.0027	−2.5713
4.00	0.0024	−2.7991
4.60	0.0020	−3.2100
5.00	0.0018	−3.5390
5.50	0.0016	−3.6477
6.00	0.0014	−3.8600
6.50	0.0014	−4.0125
7.00	0.0014	−4.1215
7.50	0.0013	−4.2077
8.00	0.0013	−4.2334
8.50	0.0013	−4.2545
9.00	0.0012	−4.2472
9.50	0.0012	−4.2158
10.00	0.0012	−4.1854

coefficient c at sites on sedimentary layers and coefficient c at KTP on the rock. As a result, we confirmed that there is a correlation between the peak period and the sedimentary layer thickness at each site in the Kathmandu Valley. Based on the relationship, the GMPE applicable to the whole Kathmandu Valley was constructed by generalizing the coefficient c obtained at each site with the equation using the bedrock depth as a parameter. Finally, we verified the applicability of the GMPE constructed in the present study.

From the above, it is suggested that the evaluation of deep underground structure is important for the evaluation of ground motion in the Kathmandu Valley because strong motion in the area is significantly amplified by thick sedimentary layers. Furthermore, improving prediction accuracy and constructing GMPEs that consider different earthquake types that occurred around Nepal are expected by accumulating strong motion records in the Kathmandu Valley in the future.

Declaration of competing interest

The authors declare that they have no known competing financial interests or personal relationships that could have appeared to influence the work reported in this paper.

CRediT authorship contribution statement

Takuho Mori: Conceptualization, Methodology, Software, Writing - original draft. **Michiko Shigefuji:** Conceptualization, Methodology, Software, Investigation, Writing - review & editing. **Subeg Bijukchhen:** Investigation, Resources, Writing - review & editing. **Tatsuo Kanno:**

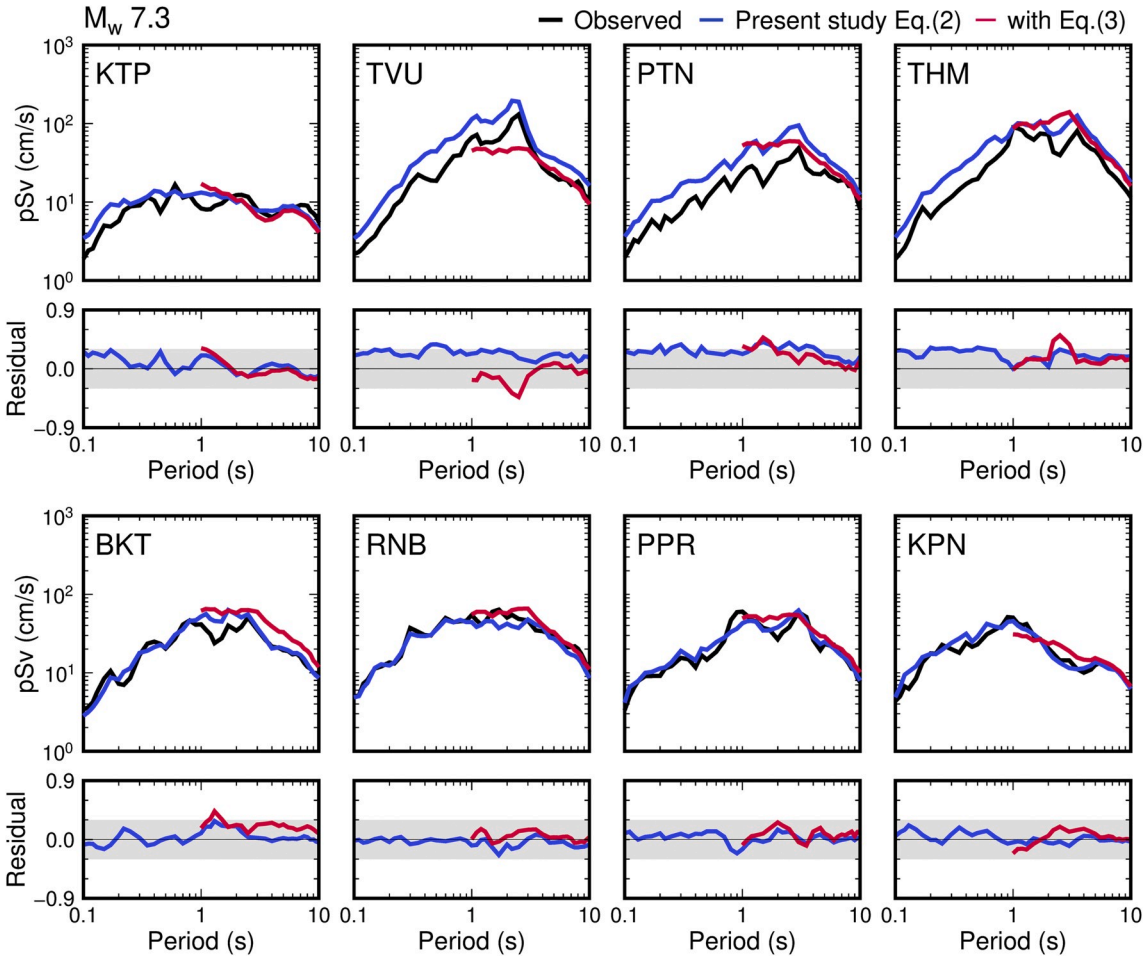

Fig. 9. Observed values of pseudo-velocity response spectra for event 5 (M_w 7.3) and values predicted by the present study (equations (2) and (3)) (upper), as well as the residuals (log [pre/obs]) (lower).

Writing - review & editing. **Nobuo Takai:** Investigation, Writing - review & editing.

Acknowledgments

The present study was supported in part by Grant-in-Aid for Scientific Research from Japan Society for the Promotion of Science (JSPS KAKENHI) Grant Numbers JP17H06215, 16K16370, and also by the Science and Technology Research Partnership for Sustainable Development (SATREPS) from Japan Science and Technology Agency (JST) / Japan International Cooperation Agency (JICA) Grant Number JPMJSA1511. We used Generic Mapping Tools (Wessel et al. [25]) for the drawing portions of the figures. We thank the reviewers for helping us significantly improve the paper.

Appendix A. Supplementary data

Supplementary data to this article can be found online at https://doi.org/10.1016/j.soildyn.2020.106208.

References

[1] Bollinger L, Sapkota SN, Tapponnier P, Klinger Y, Rizza M, Van der Woerd J, Tiwari DR, Pandey R, Bitri A, Bes de Berc S. Estimating the return times of great himalayan earthquakes in eastern Nepal: evidence from the patu and bardibas strands of the main frontal thrust. J Geophys Res: Solid Earth 2014;119:7123–63. https://doi.org/10.1002/2014jb010970.

[2] Rana BS. Mahabhukampa (the Great Earthquake) 1935.

[3] Bilham R, Wallace K. Future Mw >8 earthquakes in the Himalaya: implications form the 26th Dec 2004 Mw = 9.0 earthquake on India's eastern plate margin. Geo. Survey India Special Publ. 2005;85:1–14.

[4] Sakai H. Stratigraphic division and sedimentary facies of the Kathmandu basin group, central Nepal. J Nepal Geol Soc 2001;25:19–32.

[5] Moribayashi S, Maruo Y. Basement topography of the Kathmandu valley, Nepal - an application of gravitational method of the survey of a tectonic basin in the Himalayas. J. Japan Soc. Eng. Geo. 1980;21:30–7. https://doi.org/10.5110/jjseg.21.80.

[6] Takai N, Shigefuji M, Rajaure S, Bijukchhen S, Ichiyanagi M, Dhital MR, Sasatani T. Strong ground motion in the Kathmandu Valley during the 2015 Gorkha, Nepal, earthquake. Earth Planets Space 2016;68:10. https://doi.org/10.1186/s40623-016-0383-7.

[7] Dhakal YP, Kubo H, Suzuki W, Kunugi T, Aoi S, Fujiwara H. Analysis of strong ground motions and site effects at Kantipath, Kathmandu, from 2015 Mw 7.8 Gorkha, Nepal, earthquake and its aftershocks. Earth Planets Space 2016;68:58. https://doi.org/10.1186/s40623-016-0432-2.

[8] Kubo H, Dhakal YP, Suzuki W, Kunugi T, Aoi S, Fujiwara H. Estimation of the source process of the 2015 Gorkha, Nepal, earthquake and simulation of long-period ground motions in the Kathmandu basin using a onedimensional basin structure model. Earth Planets Space 2016;68:16. https://doi.org/10.1186/s40623-016-0393-5.

[9] Bijukchhen SM, Takai N, Shigefuji M, Ichiyanagi M, Sasatani T, Sugimura Y. Estimation of 1-D velocity models beneath strong-motion observation sites in the Kathmandu Valley using strong-motion records from moderate-sized earthquakes. Earth Planets Space 2017;69:97. https://doi.org/10.1186/s40623-017-0685-4.

[10] Bijukchhen SM. Construction of 3-D Velocity Structure Model of the Kathmandu Basin, Nepal, based on Geological Information and Earthquake Ground Motion Records. *PhD Thesis*. Hokkaido, Japan: Hokkaido University; 2018. https://doi.org/10.14943/doctoral.k13350.

[11] Singh SK, Srinagesh D, Srinivas D, Arroyo X, Pérez-Campos, Chadha RK, Suresh G, Suresh G. Strong ground motion in the indo-gangetic plains during the 2015 Gorkha, Nepal, earthquake sequence and its prediction during future earthquakes. Bull Seismol Soc Am 2017;107(3):1293–306. https://doi.org/10.1785/0120160222.

[12] Morikawa N, Fujiwara H. A new ground motion prediction equation for Japan applicable up to M9 mega-earthquake. J Disaster Res 2013;8(5).

[13] Boore DM, Stewart JP, Seyhan E, Atkinson GM. NGA-west 2 equations for predicting PGA, PGV, and 5%-damped PSA for shallow crustal earthquakes. Earthq Spectra 2014;30(3):1057–85. https://doi.org/10.1193/070113eqs184m.

[14] Takai N, Maeda T, Shigefuji M, Sasatani T. Single-site ground motion equations (SS-GMPE) of response spectra - case study for the off-sanriku outer-rise earthquakes -. J. Japan Assoc. Earthquake Eng. 2015;15(1):18–37. https://doi.org/10.5610/jaee.15.1_18 (in Japanese with English abstract).

[15] Kudo K, Kanno T, Okada H, Özel O, Erdik M, Sasatani T, Higashi S, Takahashi M, Yoshida K. Site-specific issues for strong ground motions during the Kocaeli, Turkey, earthquake of 17 August 1999, as inferred from array observations of microtremors and aftershocks. Bull Seismol Soc Am 2002;92:448–65. https://doi.org/10.1785/0120000812.

[16] Ichiyanagi M, Takai N, Shigefuji M, Bijukchhen S, Sasatani T, Rajaure S, Dhital MR, Takahashi H. Aftershock activity of the 2015 Gorkha, Nepal, earthquake determined using the Kathmandu strong motion seismographic array. Earth Planets Space 2016;68:25. https://doi.org/10.1186/s40623-016-0402-8.

[17] USGS. https://earthquake.usgs.gov/earthquakes/eventpage/us20002ejl/finite-fault. [Accessed 24 September 2019].

[18] Grandin R, Vallée M, Satriano C, Lacassin R, Klinger Y, Simoes M, Bollinger L. Rupture process of the Mw=7.9 2015 Gorkha earthquake (Nepal): insights into himalayan megathrust segmentation. Geophys Res Lett 2015;42:8373–82. https://doi.org/10.1002/2015gl066044.

[19] Aki K and Richards PG: *Quantitative Seismology: Theory and methods* 1980; W.H. Freeman and Company, San Francisco.

[20] Rajaure S, Asimaki D, Thompson EM, Hough S, Martin S, Ampuero JP, Dhital MR, Inbal A, Takai N, Shigefuji M, Bijukchhen S, Ichiyanagi M, Sasatani T, Paudel L. Characterizing the Kathmandu Valley sediment response through strong motion recordings of the 2015 Gorkha earthquake sequence. Tectonophysics 2017;714–715:146–57. https://doi.org/10.1016/j.tecto.2016.09.030.

[21] Abrahamson N, Gregor N, Addo K. BC hydro ground motion prediction equations for subduction earthquakes. Earthq Spectra 2016;32(1):23–44. https://doi.org/10.1193/051712EQS188MR.

[22] Wen K. Non-linear soil response in ground motions. Earthq Eng Struct Dynam 1994;23(6):599–608.

[23] Noguchi S, Ssasatani T, Noguchi S, Sasatani T. Quantification of degree of nonlinear site response. *14th world conference on earthquake engineering*. 2008. Beijing, paper ID: 03-03-0049.

[24] Kanno T, Narita A, Morikawa N, Fujiwara H, Fukushima Y. A new attenuation for strong ground motion in Japan based on recorded data. Bull Seismol Soc Am 2006;96:879–97. https://doi.org/10.1785/0120050138.

[25] Wessel P, Smith WHF, Scharroo R, Luis JF, Wobbe F. Generic Mapping Tools: improved version released. EOS Trans. AGU 2013;94:409–10.